RSC Advances

PAPER

View Article Online
View Journal | View Issue

Cite this: *RSC Adv.*, 2026, **16**, 9412

N-Substitution effects on the conformations of iminosugar analogues of 1-deoxy-L-idose and 1-deoxy-L-iduronic acid

Lorenzo Taglietti,[a] Eva Palomba,[b] Heiko Lange,[bd] Luca Zoia,[b] Maria Assunta Chiacchio,[c] Laura Legnani*[a] and Barbara La Ferla*[b]

Received 23rd December 2025
Accepted 7th February 2026

DOI: 10.1039/d5ra09936f

rsc.li/rsc-advances

We herein report the synthesis and complete conformational analysis of a focused library of iminosugar analogues of L-idose and L-iduronic acid designed to probe the impact of *N*-substitution on ring dynamics. Molecular modelling, supported by experimental ^{1}H NMR data, reveals that introducing alkyl or acyl substituents on the ring nitrogen profoundly alters the conformational equilibrium, inducing a clear shift from the preferred $^1C_4$ chair to the $^4C_1$ conformation. These findings highlight how targeted nitrogen functionalisation can be used to modulate the conformational landscape of iminosugars, offering new opportunities for the rational design of glycomimetic scaffolds.

Introduction

L-Iduronic acid (IdoA) is one of the main components of heparan sulfate (HS), a polysulfated glycosaminoglycan (GAG), widely present on cell surfaces and within the extracellular matrix. These polymers are involved in crucial interactions with various entities including growth factors, chemokines, and enzymes, but also viruses and bacteria, playing a pivotal role in physiological and pathological process such as cellular growth, differentiation, immune responses, angiogenesis, bacteria and virus infections.[1] The conformational flexibility of IdoA, particularly its ability to adopt multiple forms such as the chair ($^1C_4$), skew-boat ($^2S_0$), and boat conformations (Fig. 1),[2] enables specific and dynamic interactions with proteins.[3–5] This structural diversity is at the basis of the functional versatility and specificity in biological recognition processes. In particular, enzymatic recognition of IdoA residues often involves selective stabilization of specific ring conformations or conformational transitions, making conformational plasticity a key determinant of biological function.[6,7] The presence of the carboxyl group (–COOH) in L-iduronic acid strongly influences its conformational dynamics. This functional group enhances the molecule's ability to form hydrogen bonds, which are essential for bin ding to various biologically relevant proteins.

L-idose is an epimer on C5 of D-glucose and, despite its limited natural occurrence, it represents an important motif as a synthetic precursor or mimetic in the biomedical field.[8] It can adopt multiple conformations because of its flexibility around the glycosidic bond and the pyranose ring. Literature reports indicate that L-idose populates both the $^1C_4$ and $^4C_1$ conformations (Fig. 1).[9,10]

For example, α-L-iduronidase (IDUA), whose deficiency causes mucopolysaccharidosis type I (MPS I), is known to preferentially recognize IdoA residues adopting non-canonical conformations along the catalytic trajectory, including $^1C_4$ and skew-boat geometries. Similarly, bacterial heparinases and mammalian heparanases exploit the intrinsic flexibility of IdoA to stabilize specific ring puckers during substrate binding and cleavage. In this context, small molecules capable of selectively stabilizing or disfavouring particular conformations may act either as transition-state mimics or as conformational disruptors, thereby modulating enzymatic activity.[11]

Iminosugars, a subclass of glycomimetics that are structurally analogous to sugars but feature a nitrogen atom replacing the oxygen in the ring, have garnered significant attention in biomedical research due to their ability to mimic natural monosaccharides while offering enhanced stability and unique

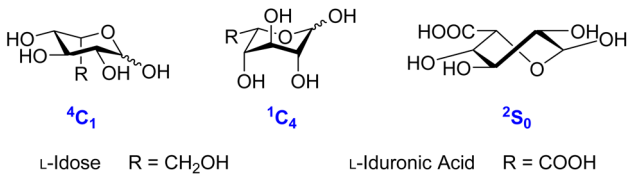

Fig. 1 Main ring conformations of L-idose and L-iduronic acid ($^1C_4$, $^4C_1$, and $^1S_0$).

[a]*Department of Biotechnology and Biosciences, University of Milano-Bicocca, Piazza della Scienza 2, 20126 Milano, Italy. E-mail: laura.legnani@unimib.it*

[b]*Department of Earth and Environmental Science, University of Milano-Bicocca, Piazza della Scienza 1, 20126 Milano, Italy. E-mail: barbara.laferla@unimib.it*

[c]*Department of Pharmaceutical and Health Sciences, University of Catania, Viale A. Doria 6, Catania, 95125, Italy*

[d]*Biochemical Process Engineering, Division of Chemical Engineering, Department of Civil, Environmental and Natural Resources Engineering, Luleå University Technology, SE-97187 Luleå, Sweden*

biological properties. These compounds are particularly valued for their potential as enzyme inhibitors, especially carbohydrate-processing enzymes like glycosidases and glycosyltransferases, making them promising candidates for applications in diverse therapeutic areas, from antiviral and anticancer, to metabolic disease treatments.[12–16]

Clinically approved iminosugars such as Miglustat and Migalastat further illustrate how subtle conformational and stereoelectronic features govern biological activity. Migalastat, in particular, acts as a pharmacological chaperone by selectively stabilizing specific folded states of α-galactosidase A, highlighting that conformational matching, rather than simple competitive inhibition, can underlie therapeutic efficacy. These examples support the hypothesis that deliberate tuning of the $^1C_4/^4C_1$ equilibrium in L-ido-configured iminosugars *via N*-substitution may represent a viable strategy to improve selectivity, potency or functional mode of action.[17]

The conformational behaviour of iminosugars is profoundly influenced by the presence and nature of substituents attached to their ring structure. Substituents, such as alkyl, acyl, or hydroxyl groups, can significantly impact the puckering of the iminosugar ring; in addition, the hybridization of the nitrogen atom impacts the conformation and the overall flexibility. These modifications are important because the biological activity of iminosugars, particularly their enzyme-inhibitory properties, are highly dependent on the precise three-dimensional conformation they adopt in solution and at the active site of target enzymes.[18–20] For example, bulky or electron-withdrawing substituents can create steric hindrance, alter the electronic properties, or modify the hybridization of the endocyclic nitrogen atom, thereby shifting the equilibrium between different conformers. The introduction of such substituents not only impacts the conformational stability of the iminosugar, but can also modulate its pharmacokinetics and pharmacodynamics, offering a pathway to fine-tune therapeutic efficacy. On this basis, we hypothesize that systematic *N*-substitution can be used to bias the $^1C_4/^4C_1$ conformational equilibrium of L-ido-configured iminosugars, thereby modulating their ability to mimic enzyme-bound conformations of L-iduronic acid and related monosaccharides. More generally, recent studies on carbohydrate-based bioactive systems have highlighted how subtle structural and conformational features can translate into pronounced biological effects, reinforcing the importance of precise conformational control in glycomimetic design.[21,22]

This article aims to investigate how different substituents attached to the ring nitrogen influence the conformational dynamics of iminosugars analogs of L-idose and L-iduronic acid. Building upon the known conformational plasticity of these monosaccharides and their importance in glycosaminoglycan–protein interactions, we sought to determine how nitrogen functionalization modulates ring puckering, conformational equilibria, and overall molecular flexibility. To this purpose we designed and synthesised a focused library of compounds that systematically vary in steric and electronic properties (Fig. 2). A comprehensive conformational analysis was then carried out through a complete modelling study at the B3LYP/6-311+G(d) level to determine all their accessible conformations and how each substituent perturbs the conformational landscape. Theoretical predictions were subsequently validated by their comparison with experimental data obtained from detailed ^1H NMR studies, providing an integrated understanding of structure-conformation relationships in these iminosugar scaffolds.

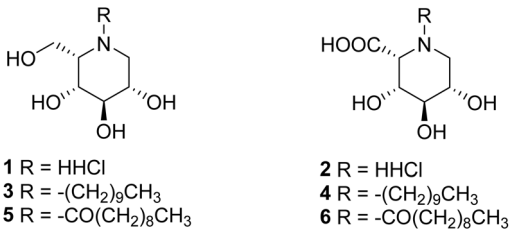

Fig. 2 Small library of IDJ (left) and IdoADJ (right) derivatives synthesized in this work.

Results and discussion

Design and synthesis

To investigate the influence of substituents on the ring nitrogen, 1-deoxy-L-idonojirimycin (IDJ) and the iminosugar analogues of 1-deoxy-L-iduronic acid (IdoADJ) were synthesised, along with their *N*-derivatives with a C10 alkyl or acyl chain (Fig. 2).

Different synthetic strategies are reported in the literature for the preparation of IDJ and IdoADJ.[18–20,23–25] For the synthesis of our focused library, we chose to start from known compound **7** (Scheme 1),[25] the perbenzylated IDJ. At first, compound **7** was converted to hydrochloric IDJ (**1**) in quantitative yield through catalytic hydrogenation (H_2, Pd/C and $Pd(OH)_2/C$).[26] For the preparation of hydrochloric IdoADJ (**2**), compound **1** was N-protected *via* $(Boc)_2O$ treatment in basic conditions (68% yield). Subsequent regioselective TEMPO-mediated oxidation of the primary alcohol was carried out by optimizing Anelli's oxidation procedure,[27–29] followed by acidic treatment to afford IdoADJ (**2**) (36% yield over the two steps).[30] The synthesis of the alkylated/acylated derivatives was achieved from *N*-debenzylated compound **8**, obtained from perbenzylated IDJ **7**, by chemoselective de-benzylation with cerium ammonium nitrate (CAN).[31] Alkylation/acylation of **8** with 1-bromodecane or decanoyl chloride afforded, respectively, benzyl-protected compounds **9** and **10** (34% and 62% yield). Subsequent debenzylation through catalytic hydrogenation provided the acylated and alkylated IDJ derivatives **3** and **5**, respectively (94% and 96% yield).

The synthesis of the corresponding oxidized compounds was accomplished using two different strategies. The acylated IdoADJ compound **6** was obtained by direct regioselective TEMPO-mediated oxidation of precursor **5**, again following the optimized Anelli procedure (36% yield). In contrast, the oxidized alkylated compound was obtained through a reductive amination approach in which precursor **4** was treated with decanal in the presence of 10% Pd/C (44% yield).

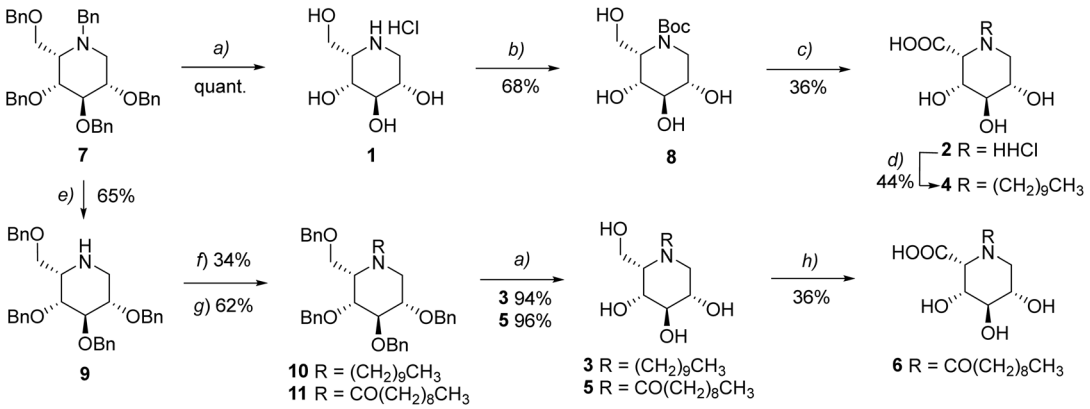

Scheme 1 Reagents and conditions: (a) H_2, Pd/C, $Pd(OH)_2$/C, cat. HCl, MeOH/DCM; (b) $(Boc)_2O$, NaOH, H_2O/dioxane, 0 °C → r.t; (c) TEMPO, NaOCl, KBr, NaOH, THF/H_2O, 0 °C then HCl 5%; (d) decanal, H_2, Pd/C, MeOH; (e) CAN, MeCN/H_2O; (f) 1-bromodecane, K_2CO_3, DMF, 80 °C; (g) decanoyl chloride, DMAP, Py; (h) TEMPO, NaOCl, KBr, NaOH, THF/H_2O, 0 °C.

Computational studies

Compounds **1–6** are iminosugars, analogues of L-iduronic acid and L-idose, respectively. While nitrogen and oxygen have very similar stereoelectronic properties, significant changes in conformational behaviour may still arise, especially when alkyl or acyl substituents are introduced on the N atom. Therefore, in order to determine their conformational preferences, a comprehensive modelling study of the target compounds was conducted through geometry optimizations within the density functional approach at the B3LYP level[32] applying the 6-311+G(d) basis set and using a polarizable continuum solvent model (PCM) in water.[33]

Moreover, NBO analysis were carried out to evaluate electronic effects driving conformational preferences (SI Fig. S2 and S3).

All degrees of conformational freedom were considered, including rotation around single bonds of the hydroxyl groups at C2, C3, and C4 as well as the different rotamers of the hydroxymethyl or carboxylic group on C5. The formation of intramolecular hydrogen bonds among the three hydroxyl moieties was also evaluated. The conformational flexibility of the ring was explored by examining the $^4C_1$ and $^1C_4$ chairs conformations as well as the accessible twisted-boat geometries. Chair conformers are the lowest-energy and most populated forms in solution, while skew-boat conformers are energetically accessible and can resemble geometries relevant for enzyme binding. True boat conformations are extremely high in energy and negligibly populated, and therefore were not considered, as their inclusion would increase computational cost without affecting solution-phase equilibria. Similarly, half-chair conformations, although important as transition-state-like geometries in retaining glycosidase catalysis, are rarely populated in solution and are thus not relevant for this study. Moreover, importantly, skew-boat conformations are widely recognized as catalytically relevant geometries in glycosidase mechanisms and are often stabilized upon enzyme binding, whereas true boat and half-chair conformations are predominantly associated with high-energy transition states and are negligibly populated in solution.[34,35] This selection of conformers efficiently captures the biologically and experimentally meaningful minima while maintaining computational efficiency. At first, the parent compounds hydrochloric IDJ (**1**) and hydrochloric IdoADJ (**2**) were modelled in their cationic form to reflect the experimental HCl salts, ensuring that the computed conformational preferences and hydrogen-bonding patterns correspond to the species present in solution.[36] The results (SI Table S1) show that the minimum energy conformers of the two compounds, **1Bb_i** and **2Bc_i** (Fig. 3) adopt the $^1C_4$ conformation. In addition, calculations (SI Table S1) show that for both compounds, there is no significant contribution of the $^4C_1$ ring conformation to the overall population. However, the relative energy of the most stable $^4C_1$ conformation of compound **1**, *i.e.*, **1Ab**, is lower (2.24 kcal mol^{-1}) than that of the most stable $^4C_1$ form **2Ac** (5.07 kcal mol^{-1}) of compound **2**.

It is important to note, however, that modelling of carbohydrates with charged groups generally yields slightly less accurate results than the modelling of the non-polar homologues. The conformational analysis was then extended to the *N*-alkyl derivatives **3** and **4** (SI Table S2), simplifying the alkyl chain to an ethyl group to reduce computational cost while maintaining stereo-electronic effects. In both cases, the N atom

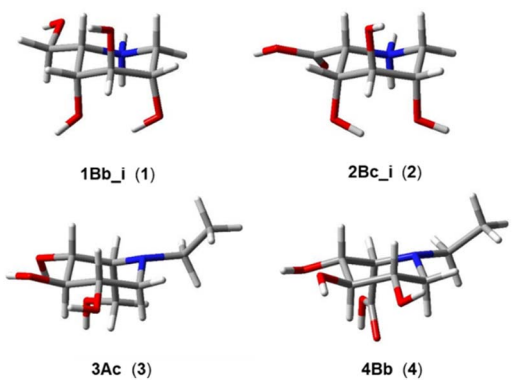

Fig. 3 3D-plots of the most stable conformations. Top row, $^1C_4$ **1Bb_i** and **2Bc_i** of compounds **1** and **2**, respectively. Bottom row, $^4C_1$ conformations **3Ac** and **4Bb** of compounds **3** and **4**, respectively, shown with the alkyl chain truncated to an ethyl moiety.

bearing the alkyl chain induces a change in the ring conformation with a complete preference for the $^4C_1$ geometry. In the case of compound **3**, two conformations are significant: the preferred **3Ac**, populated at 66.8%, and **3Ab**, which contributes for 18.5%. The other $^4C_1$ conformer does not exceed 10% of the population. Conversely, for derivative **4**, there is a greater distribution, with four conformations that exceed 10% of the population, all with the ring in the $^4C_1$ arrangement. The two most populated geometries, **4Bb** and **4Ab**, represent 40.4% and 33.3% of the population, respectively (SI Table S2). They show the mg orientation of the carboxyl group at C5, described by dihedral angle τ_4 (SI Table S2) and having the carbonyl C=O pointing underneath the ring. They only differ by the orientation of the hydroxyl groups, which in both cases form a network of H-bonds either clockwise or counterclockwise, respectively. The $^1C_4$ ring geometry does not contribute to the population for both alkyl derivatives.

To evaluate the effects of interaction with explicit water molecules, molecular dynamics (MD) simulations of compounds **3** and **4**, selected as model structures of the two series of synthesized analogues, were performed. In both cases, the complete preference for the $^4C_1$ geometry of the ring is confirmed. The data highlights that the length of the alkyl chain does not affect the ring geometry. This simplification is valid for finding a compromise between calculation times and accuracy of the results (SI Fig. S4 and S5).

Then the acylated derivatives **5** and **6** were modelled at the same DFT level of calculation. In these cases, an additional degree of conformational freedom was taken into consideration: the two possible arrangements, *Z* and *E*, around the amido moiety (Fig. 4) (SI Table S3). The two series of signals are experimentally distinguishable on the NMR timescale. In analogy to what was observed for the alkyl substituents, calculations reveal that the acyl substitution at the N atom shifts the conformational preference, confirming the transition to a $^4C_1$ ring geometry. Considering the data reported in Table S3 (SI), in the case of **5**, the *Z* and *E* series are almost equally populated (approximately 48 : 52 ratio), therefore, two distinct series of signals are expected and indeed observed in the corresponding ^{1}H-NMR spectra.

However, all the geometries described in each series with the $^4C_1$ ring conformation likely contribute to the solution equilibrium, being presumably present in a non-negligible amount. Conversely, for compound **6**, the *Z* arrangement is significantly favoured (79 : 21 ratio) with respect to the *E* one, as also observed in the ^{1}H NMR spectra. Regarding compound **5**, as specified above, the ring exhibits a $^4C_1$ geometry, showing a population distribution in which **5Bc_Z** and **5Bc_E** represent the most stable conformations. These two conformations differ in energy by only 0.09 kcal mol^{-1} with percentages of 24.4% and 21.2%, respectively. Both preferred conformations share the same orientation of substituents at C2, C3, C4, and C5, but differ in the *Z* or *E* arrangement of the amido moiety. Similarly, compound **6** displays a significant distribution of population among conformations with a $^4C_1$ ring geometry. Specifically, **6Ac_Z** and **6Bc_Z** (Fig. 4) are populated at 34.4% and 22.6%, respectively. They both feature a *trans* orientation of the carboxylic group at C5, characterized by dihedral angle τ_4 (Table S3), but differ in the clockwise (**6Ac_Z**) or counterclockwise (**6Bc_Z**) arrangement of the H-bond network involving the hydroxyl groups at C2, C3 and C4. Fig. 4 depicts the corresponding 3D-plots of the most populated conformers of **5** and **6**.

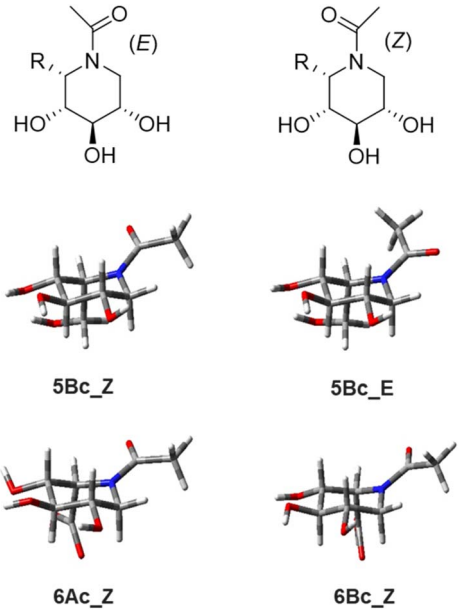

Fig. 4 Upper panel: *E* and *Z* orientation of the amido moiety of derivatives **5** and **6**. Lower panel: 3D-plots of the most represented $^4C_1$ conformations **5Bc_Z**, **5Bc_E** and **6Ac_Z**, **6Bc_Z** of compounds **5** and **6**, respectively, shown with the acyl chain truncated to an acetyl moiety.

Comparison with the conformational behaviour of the parent sugars L-idose and L-iduronic acid highlights the distinctive role of the endocyclic nitrogen in iminosugar scaffolds. In native sugars, conformational preferences are largely governed by hydroxyl orientation and, in the case of L-iduronic acid, by the presence of the carboxylate group, resulting in a predominant $^1C_4$ geometry with contributions from skew-boat conformations. In contrast, replacement of the ring oxygen with nitrogen introduces additional stereoelectronic variables, including protonation state, lone-pair orientation, and substituent-dependent steric effects, which amplify the sensitivity of the ring to substitution at the endocyclic position.[37] Consequently, *N*-substitution exerts a far more pronounced influence on ring puckering than O-substitution at peripheral hydroxyl groups, which primarily affects hydrogen-bonding and solvation.[38] The complete inversion of chair preference observed upon *N*-alkylation or *N*-acylation in the present study underscores how modification at the nitrogen atom directly reshapes the conformational landscape of L-ido-configured iminosugars, an effect that is not typically accessible through conventional O-functionalization of carbohydrates.

Spectroscopic analysis

Computational data were promptly compared with experimental spectroscopic characterization carried out through the

acquisition of ^{1}H NMR spectra. Regarding hydrochloric IDJ, (compound **1**), despite the overlapping of most proton signals, selected diagnostic signals can be interpreted. The presence of a broad H4 signal spanning approximately 6 Hz, and a visible H3 coupling constant ($J_{3,4}/J_{3,2}$ = 3.6 Hz) (SI Fig. S1) suggests a $^1C_4$ conformation, as predicted by the modelling studies. Instead, the *trans*-diaxial coupling constant between H3–H4, H3–H2 and H4–H3 (7–9 Hz) typical of a $^4C_1$ conformation, are absent. Hydrochloric IdoADJ (compound **2**), unambiguously exhibits an inverted-chair conformation, with all H-ring coupling constants below 3.6 Hz (Fig. 5). The broad triplet H3 signal at 4.11 ppm with $J_{3,4}$ = 3.4 Hz can be taken as diagnostic. Both alkylated compounds **3** and **4** display the diagnostic *trans*-diaxial coupling constants of typical $^4C_1$ conformations.

Diagnostic signals can be identified for compound **3** in H4 at 3.79 ppm and H3 at 3.52 ppm. The first is a doublet of doublets with a larger ax/ax constant of $J_{4,3}$ = 7.7 Hz and a smaller ax/eq $J_{4,5}$ = 4.6 Hz; the second is a broad triplet with an ax/ax coupling constant of 7.4 Hz. For compound **4**, the H3 triplet at 3.86 ppm with $J_{3,2} = J_{3,4}$ = 9.0 Hz clearly indicates the *trans*-diaxial orientation of H2–H3 and H3–H4. Experimental ^{1}H NMR spectra of the acylated derivatives **5** and **6** show an increased level of complexity due to the presence of two distinct orientations of the amide bond (*E* and *Z*, Fig. 4), that are slowly interconverting on the spectra acquisition time scale, leading to two partially overlapping sets of signals.

Nevertheless, diagnostic signals can be identified, and these agree with the $^4C_1$ conformation predicted by the modelling studies. For compound **5**, the diagnostic signal is the broad triplet at 3.40 ppm, assigned to H3 of the major isomer, bearing $J_{3,2} = J_{3,4}$ = 9.4 Hz (ax/ax) (Fig. 6). In compound **6**, signals are much more overlapped; nevertheless, the H4 doublet of doublets of the minor isomer at 3.54 ppm, with $J_{4,3}$ = 9.7 Hz (ax/ax) and a $J_{4,5}$ = 5.7 Hz (ax/eq), can be associated with the predicted chair conformation.

Experimental NMR data were also compared with the predicted chemical shifts (δ) of the H/C atoms of all compounds, determined through GIAO NMR calculations[39] at the B3LYP/6-311+G(d) level.

Even though in certain cases the experimental solvent was different from the one used during calculations (some of the compounds were poorly soluble in D_2O, so d_4-MeOD was employed) a good agreement was found (SI Table S4). The calculated chemical shifts also confirm the presence of two amide bond orientations in compounds **5** and **6** and predict, with good approximation, the downfield shift of proton signals that fall within the de-shielding cone of the carbonyl group. For example, the orientation of the carbonyl group in the major *E* isomer of compound **5** causes a significant downfield shift of the equatorial H1 signal, consistent with the presence of the carbonyl deshielding cone. This effect is not observed in the minor *Z* isomer, where instead the H5 proton signal falls within the carbonyl de-shielding cone, resulting in a significant 0.8 ppm downfield shift compared to the H5 signal of the *E* isomer (Fig. 5 and Table 1). Moreover, although the decyl and decanoyl chains were truncated to ethyl and ethanoyl groups for computational efficiency, the resulting conformational predictions reproduce the experimental ^{1}H-NMR chemical shifts observed for the corresponding decyl-substituted derivatives. This indicates that the primary determinants of ring puckering and hydrogen-bond networks are the nitrogen atom and its

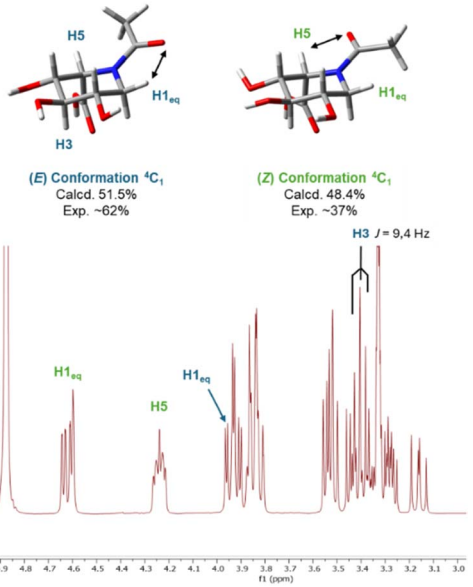

Fig. 6 Details of ^{1}H-NMR of compound **5**. Signals corresponding to the major isomer *E* are highlighted in blue, while those of the minor isomer *Z* are highlighted in green.

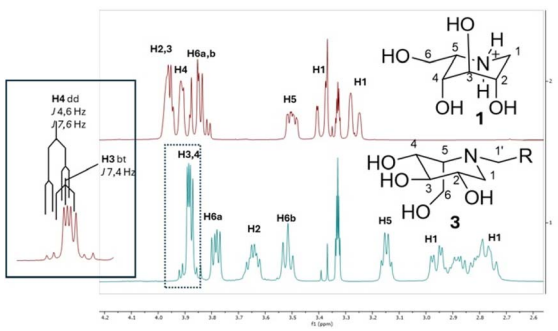

Fig. 5 Details of ^{1}H NMR direct comparison between compound **1** and alkylated compound **3**.

Table 1 Comparison between calculated and experimental chemical shifts (in ppm) of compound **5**

	$H1_{ax}$	$H1_{eq}$	H2	H3	H4	H5	H6a/H6b
***E* isomer**							
Calc.[a]	2.49	4.80	3.57	3.85	3.92	4.26	3.81/4.32
Found[b]	2.64	4.62	3.28	3.39	3.53	4.24	3.85–3.95
***Z* isomer**							
Calc.[a]	3.03	3.45	3.60	3.98	3.90	5.43	3.78/4.22
Found[b]	3.16	3.83	3.37	3.52	3.45	4.97	3.85–3.95

[a] D_2O. [b] d_4 MeOD.

immediate substituent, while chain length plays a secondary role. In this context, this validates truncated chains as a reliable, computationally efficient, and chemically meaningful strategy for probing the stereo-electronic influence of *N*-substitution on conformational equilibria.[40]

Conclusions

In conclusion, our combined experimental and computational study unambiguously establishes the preferred molecular conformations of IDJ and IdoADJ derivatives. While the parent compounds hydrochloric IDJ (**1**) and hydrochloric IdoADJ (**2**) adopt a predominant $^1C_4$ conformation in solution, mirroring the behaviour of the natural sugars L-idose and L-iduronic acid, substitution at the ring nitrogen with alkyl or acyl substituents induces a definitive shift to the $^4C_1$ chair geometry. This observed shift from $^1C_4$ to $^4C_1$ in *N*-substituted derivatives may be primarily driven by steric effects at the nitrogen, which favour an equatorial orientation of the substituent in the $^4C_1$ chair. Electronic factors, such as changes in lone-pair distribution and hyperconjugation, along with rearrangements of intramolecular hydrogen-bonding, also contribute to the stabilization of this conformation. Unlike O-substitution in native sugars, which mainly perturbs peripheral interactions, *N*-substitution in iminosugars directly alters the electronic and steric environment of the ring, enabling deliberate control over chair preference and conformational flexibility. This behaviour, consistently supported by both ^{1}H NMR analysis and DFT calculations, provides a crucial structural insight for the rational design of new iminosugar-based molecules with potential biological activity. Our findings underscore the relevance of nitrogen substitution in modulating ring flexibility and can guide the development of novel glycomimetics that retain the core L-ido stereochemistry while enabling precise tuning of ring conformation to optimize interactions with biological targets.

Experimental

General experimental methods

Commercially available chemicals were used as purchased without purification. Reactions were performed in dried glassware equipped with a magnetic stir bar and were monitored by thin layer chromatography (TLC) using commercial aluminum-backed silica gel plates (Merck, Kieselgel 60 F254) or glass-backed silica gel plates (Merck, Kieselgel 60 F254). TLC spots were visualized under ultraviolet light (254 nm) and by heating the plate after treatment with a $KMnO_4$ spray (3% solution of $KMnO_4$ in 10% aqueous potassium hydroxide (w/v)), or cerium molybdate spray (solution of $(NH_4)_6Mo_7O_{24}\cdot H_2O$ (25 g L^{-1}) and $(NH_4)_4Ce(SO_4)_4\cdot 2H_2O$ (10 g L^{-1}) in 10% aqueous sulfuric acid), or H_2SO_4 spray (5% v/v H_2SO_4 in ethanol, or ninhydrin spray (0.5% (w/v) ninhydrin in ethanol). Standard inert atmosphere techniques were used in handling all air- and moisture-sensitive reagents. Unless otherwise stated, reactions were performed under a positive pressure of dry argon or nitrogen. Product purification by flash column chromatography was performed using a Merck silica gel 60 Å (35–70 μm mesh). ^{1}H and ^{13}C NMR spectra were recorded on Bruker Avance 400 MHz or Bruker Avance 600 MHz spectrometers. Proton and carbon signal assignments were established using COSY and HSQC experiments. High-resolution mass spectra (HRMS) were recorded on a Xevo G2-XS q-TOF mass spectrometer. Piperidine **7** (see Scheme 1) was prepared as previously published.[25]

Computational methods

All calculations were carried out using the Gaussian16 program Package[41] through optimizations in water using a self-consistent reaction field (SCRF) method, based on the polarizable continuum model (PCM)[26] at the B3LYP/6-311+G(d) level.[32] A large number of initial geometries were prepared and optimized, varying in the $^1C_4$ or $^4C_1$ conformations of the ring, as well as in the orientation of all substituents. Their respective contributions to the overall population were determined at 298 K using the Boltzmann equation. The values of torsional angles, relative energies and percentage contributions of the identified conformations of compounds **1–6** are reported in the supportings (SI Tables S1, S2, S3a and S3b). Vibrational frequencies were computed to verify that the optimized structures were minimal. The theoretical ^{1}H NMR chemical shifts for all compounds were determined through GIAO NMR calculations[39] at the same level already used for the optimizations. The obtained values were weighted averages based on the population percentages of the identified geometries.

Synthesis and characterization

General procedure GP1 for hydrogenation/hydrogenolysis. To a solution of compound **7**, **9**, or **10** in a dry methanol and dry dichloromethane 1 : 1 mixture (0.25 M) were added 10% Pd/C (15% w/w relative to the starting material), 10% $Pd(OH)_2$/C (15% w/w relative to the starting material) and aqueous 37% HCl (cat. amount) for compounds **7** and **9**, or glacial acetic acid (cat. amount) for compound **10**. The suspension was hydrogenated at room temperature for 16 h and then filtered through a Celite® pad. The filter cake was rinsed with methanol, and the combined filtrate and washings were concentrated under reduced pressure to obtain pure compound **1**. The residue was purified with flash column chromatography (EtOAc/MeOH 8 : 2) to give pure polyhydroxylated compounds **3** and **5**.

*Compound **1**.* The title compound was prepared according to GP1 from perbenzylated piperidine **7** (311.4 mg, 0.507 mmol) to give pure **1** as a white solid (101.2 mg, 0.507 mmol, quantitative yield); ^{1}H NMR (400 MHz, CD_3OD) δ 3.99–3.91 (m, 2H, H-2, H-3), 3.89 (dd, $J = 3.6$, 1.7 Hz, 1H, H-4), 3.87–3.78 (m, 2H, H-6a, H-6b), 3.48 (ddd, $J = 9.0$, 5.0, 1.9 Hz, 1H, H-5), 3.42–3.33 (m, 1H, H-1a), 3.29–3.20 (m, 1H, H-1b). ^{13}C NMR (101 MHz, CD_3OD) δ 69.21, 68.36, 67.85 (C-2), 60.65 (C-6), 58.28 (C-5), 47.01 (C-1). HRMS (ESI^+): calcd. for $C_6H_{14}NO_4$ $[M + H]^+$ m/z 164.0923; found m/z 164.0927.

*Compound **8**.* Triol **1** (104.9 mg, 0.526 mmol) was dissolved in a water and 1,4-dioxane 1 : 1 mixture (4 mL, 0.13 M) and cooled on ice. $(Boc)_2O$ (344.1 mg, 1.577 mmol, 3 equiv.) and 1 M aqueous NaOH were then added to reach pH ~ 9–10. The

resulting mixture was warmed up to room temperature and stirred overnight. The reaction was then quenched with sat. NH_4Cl (0.5 mL), concentrated under reduced pressure and the crude purified by flash chromatography ($CHCl_3$/MeOH 85 : 15) to afford pure **8** as a white solid (94.6 mg, 0.359 mmol, 68% yield). ^{1}H NMR (400 MHz, CD_3OD) δ 4.43 (bs, 1H), 4.09 (bs, 1H), 3.91–3.83 (m, 1H), 3.77 (dd, J = 11.9, 9.4 Hz, 1H), 3.49 (dd, J = 9.7, 6.1 Hz, 1H), 3.41 (t, J = 9.2 Hz, 1H), 3.36–3.32 (m, 1H), 2.92–2.73 (m, 1H), 1.47 (s, 9H). ^{13}C NMR (101 MHz, CD_3OD) δ 157.15, 81.52, 76.36, 72.49, 71.66, 59.03, 57.80, 28.59. HRMS (ESI^+): calcd. for $C_{11}H_{21}NO_6Na$ $[M + Na]^+$ m/z 286.1267; found m/z 286.1269. HRMS (ESI^-): calcd. for $C_{11}H_{21}NO_6Cl$ $[M + Cl]^-$ m/z 298.1057; found m/z 298.1058. HRMS (ESI^-): calcd. for $C_{12}H_{22}NO_8$ $[M + FA^- H]^-$ m/z 308.1345; found m/z 308.1346.

General procedure GP2 for oxidation. To a solution of compound **8**, or **5** dissolved in a water and tetrahydrofuran 1 : 1 mixture (0.1 M) at 0 °C were added TEMPO (cat. amount), aqueous 6–14% NaOCl (2.2 equiv.), KBr (0.5 equiv.) and 1 M aqueous NaOH to reach pH ~10–11. The reaction mixture was stirred at 0 °C for 5 h, quenched with 1 M aqueous $Na_2S_2O_3$ and concentrated under reduced pressure.

*Compound **2**.* N-Boc protected compound **8** (42.2 mg, 0.160 mmol) was oxidized according to GP2. The crude was filtered on silica EtOAc/MeOH/H_2O 80 : 20 : 0 → 80 : 20 : 5) to give a white solid (15.8 mg) used for the subsequent step. The solid was co-evaporated under reduced pressure with aqueous 5% HCl (3 × 3 mL) and then with H_2O (3 × 3 mL) to afford pure compound **2** as a white solid (12.2 mg, 36% yield over two steps). ^{1}H NMR (400 MHz, D_2O) δ 4.43–4.37 (m, 1H, H-5), 4.30 (d, J = 2.3 Hz, 1H, H-4), 4.11 (t, J = 3.4 Hz, 1H, H-3), 4.10–4.03 (m, 1H, H-2), 3.51–3.38 (m, 2H, H-1a, H-1b). ^{13}C NMR (151 MHz, D_2O) δ 171.09 (C-6), 68.37, 67.22, 65.74, 57.81, 45.09 (C-1). HRMS (ESI^+): calcd. for $C_6H_{12}NO_5$ $[M + H]^+$ m/z 178.0715; found m/z 178.0719.

*Compound **4**.* To a solution of compound **2** (10.3 mg, 0.048 mmol) in dry MeOH (1.5 mL) were added 10% Pd/C (cat. amount) and decanal (11 μL, 0.058 mmol, 1.2 equiv.), and the mixture was hydrogenated at room temperature for 16 h. The suspension was then filtered through Celite pad. The filter cake was rinsed with MeOH, and the combined filtrate and washings were concentrated under reduced pressure. The reaction crude was purified by flash chromatography (AcOEt/MeOH/H_2O 80 : 20 : 0 → 80 : 20 : 5) to give pure **4** as a white solid (6.7 mg, 0.021 mmol, 44% yield). ^{1}H NMR (600 MHz, D_2O, 310 K) δ 3.86 (t, J = 9.0 Hz, 1H, H-3), 3.70–3.65 (m, 1H, H-2), 3.64 (d, J = 6.0 Hz, 1H, H-5), 3.62–3.57 (m, 1H, H-4), 3.10 (t, J = 10.8 Hz, 1H, H-1a), 2.91–2.86 (m, 1H, H-1b), 2.73–2.67 (m, 1H, NCH), 2.66–2.59 (m, 1H, NCH), 1.62–1.47 (m, 2H, NCH_2CH_2), 1.33 (bs, 14H, Chain), 0.98–0.79 (bt, 3H, -CH_3). ^{13}C NMR (151 MHz, D_2O, 310 K, extrapolated from HSQC) δ 80.57 (C-3), 77.99 (C-2), 76.23 (C-4), 72.51 (C-5), 61.05 (N–C), 57.92 (C-1), 32.37, 35.02, 19.67 (COOH not visible in HSQC). HRMS (ESI^+): calcd. for $C_{16}H_{32}NO_5$ $[M + H]^+$ m/z 318.2280; found m/z 318.2290. HRMS (ESI^-): calcd. for $C_{16}H_{30}NO_5$ $[M - H]^-$ m/z 316.2124; found m/z 316.2124.

*Compound **9**.* Ceric ammonium nitrate (CAN) (11.12 g, 20.28 mmol, 2.1 equiv.) was added portion wise to a stirred solution of compound 7 (5.93 g, 9.66 mmol) in a MeCN/H_2O mixture (5 : 1, 100 mL) and stirred at room temperature for 16 h. The reaction was then quenched by the addition of saturated aqueous $NaHCO_3$ (20 mL) and stirred vigorously for ten minutes before extracting with EtOAc (3 × 100 mL). The combined organic layers were dried over anhydrous Na_2SO_4 and concentrated under reduced pressure. The crude extract was purified by flash chromatography (EtOAc/PE 9 : 1) to give pure **9** as a pale-yellow oil (1.92 g, 3.67 mmol, 38% yield, 65% based on recovered starting material). ^{1}H NMR (400 MHz, $CDCl_3$) δ 7.36–7.18 (m, 20H, HAr), 4.63–4.60 (m, 2H, 2C*H*Ph), 4.59–4.53 (m, 3H, 3CHPh), 4.53–4.45 (m, 3H, 3CHPh), 3.70–3.58 (m, 3H, H-3, H-6a, H6b), 3.53 (dd, J = 9.5, 5.4 Hz, 1H, H-4), 3.47–3.41 (m, 1H, H-2), 3.40–3.34 (m, 1H, H-5), 3.00 (dd, J = 13.0, 4.0 Hz, 1H, H-1a), 2.87 (dd, J = 12.9, 6.5 Hz, 1H, H-1b), 2.70 (s, 1H, NH). ^{13}C NMR (101 MHz, $CDCl_3$) δ 138.54, 138.49, 138.38, 138.27, 128.40, 128.35, 128.30, 127.90, 127.80, 127.75, 127.67, 127.62, 127.58, 77.33, 77.01, 76.70, 74.01, 73.37, 72.61, 72.06, 67.14, 54.54, 44.09. HRMS (ESI^+): calcd. for $C_{34}H_{38}NO_4$ $[M + H]^+$ m/z 524.2801; found m/z 524.2802.

*Compound **10**.* To a solution of compound **9** (446.7 mg, 0.853 mmol) in dry DMF (5 mL) was added K_2CO_3 (294.9 mg, 2.13 mmol, 2.5 equiv.) and 1-bromodecane (0.195 mL, 0.938 mmol, 1.1 equiv.). The resulting mixture was stirred overnight at 80 °C under argon atmosphere. The reaction mixture was then cooled down to room temperature, quenched with H_2O (10 mL), extracted with EtOAc and concentrated under reduced pressure. The residue was purified by flash chromatography (PE/EtOAc 9 : 1) to afford the product **10** as a yellow oil (193.0 mg, 0.291 mmol, 34% yield). ^{1}H NMR (400 MHz, $CDCl_3$) δ 7.39–7.23 (m, 20H, HAr), 4.90–4.77 (m, 2H, 2CHPh), 4.76–4.61 (m, 4H, 4CHPh), 4.58–4.46 (m, 2H, 2CHPh), 3.83 (dd, J = 10.1, 6.4 Hz, 1H), 3.76–3.64 (m, 2H), 3.62–3.47 (m, 2H), 3.38 (td, J = 6.2, 2.5 Hz, 1H, H-5), 2.89 (dd, J = 11.9, 5.4 Hz, 1H), 2.71 (ddd, J = 12.4, 9.0, 6.2 Hz, 1H), 2.58–2.47 (m, 2H, N(CH_2)-R), 1.52–1.37 (m, 2H, NCH_2CH_2), 1.32–1.23 (m, 14H, Chain), 0.90 (t, 3H, -CH_3). ^{13}C NMR (101 MHz, $CDCl_3$) δ 139.17, 138.70, 138.64, 138.58, 128.37, 128.31, 128.26, 127.96, 127.79, 127.60, 127.52, 127.45, 127.40, 83.12, 80.29, 78.90, 77.36, 77.04, 76.72, 75.35, 73.25, 73.04, 72.69, 64.40, 59.70, 54.78, 49.89, 31.95, 29.70, 29.64, 29.57, 29.38, 28.00, 27.30, 22.72, 14.15. HRMS (ESI^+): calcd. for $C_{44}H_{58}NO_4$ $[M + H]^+$ m/z 664.4366; found m/z 664.4366.

*Compound **11**.* To a solution of compound **9** (473.0 mg, 0.903 mmol) in dry pyridine (4.5 mL, 0.5 M) were added DMAP (cat. amount) and decanoyl chloride (0.33 mL, 1.54 mmol, 1.7 equiv.). The resulting mixture was stirred overnight at room temperature under argon atmosphere. The reaction mixture was then quenched with MeOH (3 mL). The mixture was transferred to a separatory funnel and diluted with EtOAc (50 mL). The organic phase was washed with 5% aqueous HCl (3 × 10 mL), followed by brine (10 mL). The organic layer was dried over Na_2SO_4, filtered, and concentrated under reduced pressure. The residue was purified by flash chromatography (PE/EtOAc 9 : 1) to obtain the product **11** as a yellow oil (379.8 mg, 0.560 mmol, 62% yield). ^{1}H NMR (400 MHz, $CDCl_3$) δ 7.34–7.16 (m, 40H, HAr), 5.23 (td, J = 7.1, 3.4 Hz, 1H, H-5), 4.87–4.82 (m, 1H), 4.82–4.36 (m, 16H, 16CHPh), 4.14–4.06 (m, 1H, H-5′), 3.86–3.71 (m, 3H), 3.64 (ddd, J = 9.9, 6.3, 2.7 Hz, 2H), 3.58–3.50 (m,

2H), 3.45 (ddd, J = 15.6, 9.6, 6.3 Hz, 2H), 3.31 (dddd, J = 16.5, 11.2, 8.7, 5.6 Hz, 2H), 3.14 (dd, J = 13.3, 11.2 Hz, 1H), 2.49 (dd, J = 13.5, 11.1 Hz, 1H), 2.31–2.24 (m, 1H), 2.21 (dd, J = 9.2, 6.3 Hz, 1H), 2.16–1.97 (m, 3H), 1.52–1.37 (m, 4H), 1.28–1.17 (m, 24H), 0.86–0.80 (m, 6H). ^{13}C NMR (101 MHz, $CDCl_3$) δ 173.39, 172.63, 138.81, 138.71, 138.22, 138.17, 138.04, 137.92, 137.87, 129.76, 128.56, 128.54, 128.46, 128.39, 128.35, 128.32, 128.11, 128.07, 128.04, 127.96, 127.90, 127.86, 127.78, 127.74, 127.71, 127.61, 127.57, 127.52, 127.36, 82.70, 82.49, 79.01, 78.90, 78.34, 78.06, 77.37, 77.05, 76.73, 75.67, 75.63, 73.80, 73.56, 73.31, 73.00, 72.87, 72.83, 66.18, 64.77, 55.71, 49.02, 44.49, 38.49, 33.88, 33.58, 33.23, 31.91, 31.86, 29.53, 29.50, 29.46, 29.41, 29.37, 29.33, 29.27, 29.10, 25.32, 25.30, 24.77, 22.70, 14.13, 14.12. HRMS (ESI$^+$): calcd. for $C_{44}H_{56}NO_5$ $[M + H]^+$ m/z 678.4158; found m/z 678.4159. HRMS (ESI$^+$): calcd. for $C_{44}H_{55}NO_5Na$ $[M + Na]^+$ m/z 700.3978; found m/z 700.3975.

Compound 3. The title compound was prepared according to GP1 from perbenzylated piperidine **10** (173.0 mg, 0.261 mmol) to give pure **3** as a white solid (74,4 mg, 0.245 mmol, 94% yield). ^{1}H NMR (400 MHz, CD_3OD) δ 3.91–3.81 (m, 2H, H-3, H-4), 3.77 (dd, J = 7.7, 4.5 Hz, 1H, H-6a), 3.63 (td, J = 7.7, 4.4 Hz, 1H, H-2), 3.50 (t, J = 7.4 Hz, 1H, H-6b), 3.13 (q, J = 5.1 Hz, 1H, H-5), 2.98–2.83 (m, 2H, H-1a, H-1b), 2.77 (ddt, J = 16.5, 12.3, 7.1 Hz, 2H, N(CH_2)-R), 1.58 (tdd, J = 12.4, 6.5, 3.5 Hz, 2H, N(CH_2)-(CH_2)-R)), 1.36–1.27 (m, 14H, Chain), 0.92–0.87 (m, 3H, -CH_3). ^{13}C NMR (101 MHz, CD_3OD) δ 74.22, 72.60, 70.70, 63.96, 58.32, 55.44, 53.13, 49.64, 49.43, 49.21, 49.00, 48.79, 48.57, 48.36, 33.05, 30.72, 30.68, 30.56, 30.44, 28.25, 27.43, 23.72, 14.44. HRMS (ESI$^+$): calcd. for $C_{16}H_{34}NO_4$ $[M + H]^+$ m/z 304.2488; found m/z 304.2489. HRMS (ESI$^-$): calcd. for $C_{16}H_{33}NO_4Cl$ $[M + Cl]^-$ m/z 338.2098; found m/z 338.2099. HRMS (ESI$^-$): calcd. for $C_{17}H_{34}NO_6$ $[M + FA - H]^-$ m/z 348.2386; found m/z 348.2388.

Compound 5. The title compound was prepared according to GP1 from perbenzylated piperidine **11** (349.8 mg, 0.516 mmol) to give pure **5** as a white solid (157.8 mg, 0.497 mmol, 96% yield). ^{1}H NMR (400 MHz, CD_3OD) δ 4.95 (dddd, J = 10.6, 5.9, 4.3, 1.3 Hz, 1H, H-5), 4.60 (ddd, J = 13.4, 5.7, 1.3 Hz, 1H), 4.29–4.16 (m, 1H, H5), 3.91 (ddd, J = 12.0, 10.4, 4.1 Hz, 2H), 3.81 (ddd, J = 12.0, 9.6, 2.2 Hz, 3H), 3.58–3.47 (m, 2H), 3.45–3.33 (m, 3H), 3.29–3.22 (m, 1H), 3.14 (dd, J = 13.7, 11.1 Hz, 1H), 2.62 (dd, J = 13.4, 11.1 Hz, 1H), 2.57–2.38 (m, 4H), 1.61 (qd, J = 7.9, 3.6 Hz, 4H), 1.36–1.27 (m, 24H), 0.93–0.88 (m, 6H). ^{13}C NMR (101 MHz, CD_3OD) δ 174.47, 174.15, 74.91, 74.82, 71.36, 70.69, 69.81, 59.76, 56.54, 55.73, 54.36, 45.35, 40.31, 33.26, 32.97, 31.65, 29.24, 29.17, 29.10, 29.07, 29.03, 25.27, 25.25, 22.33, 13.03. HRMS (ESI$^+$): calcd. for $C_{16}H_{32}NO_5$ $[M + H]^+$ m/z 318.2280; found m/z 318.2284. HRMS (ESI$^+$): calcd. for $C_{16}H_{31}NO_5Na$ $[M + Na]^+$ m/z 340.2100; found m/z 340.2103. HRMS (ESI$^-$): calcd. for $C_{16}H_{31}NO_5Cl$ $[M + Cl]^-$ m/z 352.1891; found m/z 352.1894. HRMS (ESI$^-$): calcd. for $C_{17}H_{32}NO_7$ $[M + FA - H]^-$ m/z 362.2182; found m/z 362.2182.

Compound 6. The title compound was prepared according to GP2 from *N*-decanoyl piperidine **5** (28.1 mg, 0.107 mmol) to give pure **6** as a white solid (10.5 mg, 0.038 mmol, 36% yield). ^{1}H NMR (400 MHz, D_2O) δ 5.25–5.18 (m, 1H, H5), 4.73–4.67 (m, 1H, H5′), 4.58–4.48 (m, 1H, H-1′a), 4.08–3.99 (m, 1H, H-1a), 3.68–3.43 (m, 4H), 3.31–3.21 (m, 2H), 3.09 (dd, J = 13.8, 10.7 Hz, 1H, H-1b), 2.71–2.39 (m, 3H), 1.69–1.58 (m, 4H), 1.50–1.21 (m, 28H, Chain), 0.90 (t, 6H, -CH_3). ^{13}C NMR (101 MHz, D_2O) δ 176.72, 176.21, 169.99, 169.95, 76.13, 76.02, 71.34, 70.51, 69.52, 68.77, 59.21, 54.81, 47.18, 46.74, 43.15, 32.92, 31.15, 28.55, 28.52, 24.97, 22.05, 13.46, 8.33. HRMS (ESI$^+$): calcd. for $C_{16}H_{30}NO_6$ $[M + H]^+$ m/z 332.2062; found m/z 332.2062.

Author contributions

Conceptualization, B. L. F. and L. L.; methodology, B. L. F. and L. L.; investigation, L. T. and E. P.; resources, B. L. F., H. L., L. Z. and M. A. C.; writing, B. L. F., L. L. and L. T.; project administration, B. L. F. and L. L. All authors have read and agreed to the published version of the manuscript.

Conflicts of interest

There are no conflicts to declare.

Data availability

The data supporting this article have been included as part of the supplementary information (SI). Supplementary information: experimental details, computational calculations, NMR for all new compounds. See DOI: https://doi.org/10.1039/d5ra09936f.

Acknowledgements

Project funded under the National Recovery and Resilience Plan (PNRR), Mission 4 Component 2 Investment 1.1 – Call for tender No. 104 of 02.02.2022 of Italian Ministry of University and Research funded by the European Union – NextGenerationEU. Award Number: Project code 2022No.9E847, Concession Decree No. 1064 of 18.07.2023 adopted by the Italian Ministry of the University and Research, CUP H53D23004630006 Multifunctional compounds for a multitarget approach against neurodegenerative disorders – MULTIFUN.

Notes and references

1 S. A. Brooks, M. V. Dwek and U. Schumacher, *Functional and Molecular Glycobiology*, BIOS, Oxford, 2002.
2 P. Oborský, I. Tvaroska, B. Kralová and V. Spiwokdx, *J. Phys. Chem. B*, 2013, **117**, 1003–1009.
3 J. Kreuger, D. Spillmann, J. P. Li and U. Lindahl, *J. Cell Biol.*, 2006, **174**, 323–327.
4 C. Noti and P. H. Seeberger, *Chem. Biol.*, 2005, **12**, 731–756.
5 J. C. Muñoz-García, J. López-Prados, J. Angulo, I. Díaz-Contreras, N. Reichardt, J. L. de Paz, M. Martín-Lomas and P. M. Nieto, *Chem. Eur. J.*, 2012, **18**, 16319–16331.
6 D. R. Ferro, A. Provasoli, M. Ragazzi, B. Casu, G. Torri, V. Bossennec, B. Perly, P. Sinaÿ, M. Petitou and J. Choay, *Carbohydr. Res.*, 1990, **195**, 157–167.
7 M. Guerrini, S. Guglieri, D. Beccati, G. Torri, C. Viskov and P. Mourier, *Biochem. J.*, 2006, **399**, 191–198.

8 R. Raigawali, S. Anand, A. Chandra, V. Mahida, P. R. Bhoge, J. N. Abrahama and R. Kikkeri, *Chem. Commun.*, 2025, **61**, 8552–8555.
9 O. Guvench, D. Martin and M. Greene, *Int. J. Mol. Sci.*, 2022, **23**, 473.
10 B. Bose-Basu, W. Zhang, J. L. W. Kennedy, M. J. Hadad, I. Carmichael and A. S. Serianni, *J. Org. Chem.*, 2017, **82**, 1356–1370.
11 C. D. Shanthamurthy, A. Gimeno, S. Leviatan Ben-Arye, N. V. Kumar, P. Jain, V. Padler-Karavani, J. Jiménez-Barbero and R. Kikkeri, *ACS Chem. Biol.*, 2021, **16**, 2481–2489.
12 N. Asano, R. J. Nash, R. J. Molyneux and G. W. J. Fleet, *Tetrahedron: Asymm.*, 2000, **11**, 1645–1680.
13 (*a*) A. E. Stütz, *Iminosugars as Glycosidase Inhibitors: Nojirimycin and beyond*, Wiley-VCH, Weinheim, Germany, 1999; (*b*) P. Greimel, J. Spreitz, A. E. Stutz and T. M. Wrodnigg, *Curr. Topics Med. Chem.*, 2003, **3**, 513–523.
14 J. Alper, *Science*, 2001, **291**, 2338–2343.
15 D. Pavlovič, D. C. A. Neville, O. Argaud, B. Blumberg, R. A. Dwek, W. B. Fischer and N. Zitzmann, *Proc. Natl. Acad. Sci. U. S. A.*, 2003, **100**, 6104–6108.
16 A. Orsato, E. Barbagallo, B. Costa, S. Olivieri, L. De Gioia, F. Nicotra and B. La Ferla, *Eur. J. Org Chem.*, 2011, 5012–5019.
17 G. Parenti, G. Andria and K. J. Valenzano, *Mol. Ther.*, 2015, **23**, 1138–1148.
18 N. J. Pawar, V. S. Parihar, S. T. Chavan, R. Joshi, P. V. Joshi, S. G. Sabharwal, V. G. Puranik and D. D. Dhavale, *J. Org. Chem.*, 2012, **77**, 7873–7882.
19 D. D. Dhavale, M. M. Matin, T. Sharmab and S. G. Sabharwalb, *Bioorg. Med. Chem.*, 2003, **11**, 3295–3305.
20 W. Schönemann, E. Gallienne, P. Compain, K. Ikeda, N. Asano and O. R. Martin, *Bioorg. Med. Chem.*, 2010, **18**, 2645–2650.
21 A. Tamburrini, C. Colombo and A. Bernardi, *Med. Res. Rev.*, 2019, **40**, 495–531.
22 H. Gong, X. Tan, J. Hou, Z. Gong, X. Qin, J. Nie, H. Zhu and S. Zhong, *Int. J. Biol. Macromol.*, 2024, **282**, 137232.
23 N. N. Saha, V. N. Desai and D. D. Dhavale, *Tetrahedron*, 2001, **57**, 39–46.
24 J. Désiré, Z. Debbah, D. Gueyrard, J. Marrot, Y. Blériot and A. Kato, *Carbohydr. Res.*, 2023, **532**, 108903.
25 P. A. Fowler, A. H. Haines, R. J. K. Taylor, E. J. T. Chrystal and M. B. Gravestock, *Carbohydr. Res.*, 1993, **246**, 377–381.
26 Y. Li, G. Manickam, A. Ghoshal and P. Subramaniam, *Synth. Commun.*, 2006, **36**, 925–928.
27 P. Lucio Anelli, C. Biffi, F. Montanari and S. Quici, *J. Org. Chem.*, 1987, **52**, 2559–2562.
28 G. Tojo and M. Fernández, Oxidation of Primary Alcohols to Carboxylic Acids A Guide to Current Common Practice in *Basic Reactions in Organic Synthesis Series*, ed. G. Tojo, Springer, 2007.
29 M. Artola, C. L. Kuo, S. A. McMahon, V. Oehler, T. Hansen, M. van der Lienden, X. He, H. van den Elst, B. I. Florea, A. R. Kermode, G. A. van der Marel, T. M. Gloster, J. D. C. Codée, H. S. Overkleeft and J. M. F. G. Aerts, *Chem. Eur. J.*, 2018, **24**, 19081–19088.
30 G. G. Doherty, G. J. M. Ler, N. Wimmer, P. V. Bernhardt, R. A. Ashmus, D. J. Vocadlo, Z. Armstrong, G. J. Davies, M. Maccarana, J. Li, Y. Kayal and V. Ferro, *ChemBioChem*, 2023, **24**, e202200619.
31 S. D. Bull, S. G. Davies, C. Fenton, A. W. Mulvaney, R. Shyam Prasad and A. D. Smith, *J. Chem. Soc. Perkin*, 2000, **1**, 3765–3774.
32 (*a*) A. D. Becke, *J. Chem. Phys.*, 1993, **98**, 5648–5652; (*b*) C. Lee, W. Yang and R. G. Parr, *Phys. Rev. B:Condens. Matter Mater. Phys.*, 1988, **37**, 785.
33 V. Barone, M. Cossi and J. Tomasi, *J. Comput. Chem.*, 1998, **19**, 404–417.
34 A. Ardèvol and C. Rovira, *J. Am. Chem. Soc.*, 2015, **137**, 7528–7547.
35 D. J. Vocadlo and G. J. Davies, *Curr. Opin. Chem. Biol.*, 2008, **12**, 539–555.
36 In the case of L-idose, the 1C4 and 4C1 conformations prefer the alpha configuration at C1 with a ΔG of 1.64 kcal mol^{-1}. For iduronic acid, the 1C4 prefers the alpha configuration at C1 and 4C1 the beta one with a ΔG of 0.28 kcal mol^{-1}. In particular in the case of iduronic acid, the substitution of the O atom with the N one in the ring definitively favors the 4C1 conformation.
37 D. Heightman and A. T. Vasella, *Angew. Chem., Int. Ed.*, 1999, **38**, 750–770.
38 B. Mulloy and M. J. Forster, *Glycobiology*, 2000, **10**, 1147–1156.
39 (*a*) K. Wolinski, F. James, J. F. Hinton and P. Pulay, *J. Am. Chem. Soc.*, 1990, **112**, 8251–8260; (*b*) R. Ditchfield, *Mol. Phys.*, 1974, **27**, 789–807.
40 D. Colombo, P. Ferraboschi, P. Grisenti and L. Legnani, *Magn. Reson. Chem.*, 2007, **46**, 99–102.
41 M. J. Frisch, G. W. Trucks, H. B. Schlegel, G. E. Scuseria, M. A. Robb, J. R. Cheeseman, G. Scalmani, V. Barone, G. A. Petersson, H. Nakatsuji, X. Li, M. Caricato, A. V. Marenich, J. Bloino, B. G. Janesko, R. Gomperts, B. Mennucci, H. P. Hratchian, J. V. Ortiz, A. F. Izmaylov, J. L. Sonnenberg, D. Williams-Young, F. Ding, F. Lipparini, F. Egidi, J. Goings, B. Peng, A. Petrone, T. Henderson, D. Ranasinghe, V. G. Zakrzewski, J. Gao, N. Rega, G. Zheng, W. Liang, M. Hada, M. Ehara, K. Toyota, R. Fukuda, J. Hasegawa, M. Ishida, T. Nakajima, Y. Honda, O. Kitao, H. Nakai, T. Vreven, K. Throssell, J. A. Montgomery Jr, J. E. Peralta, F. Ogliaro, M. J. Bearpark, J. J. Heyd, E. N. Brothers, K. N. Kudin, V. N. Staroverov, T. A. Keith, R. Kobayashi, J. Normand, K. Raghavachari, A. P. Rendell, J. C. Burant, S. S. Iyengar, J. Tomasi, M. Cossi, J. M. Millam, M. Klene, C. Adamo, R. Cammi, J. W. Ochterski, R. L. Martin, K. Morokuma, O. Farkas, J. B. Foresman, D. J. Fox, *Gaussian 16, R. C. 01*, Gaussian, Inc., Wallingford CT, 2016.